Using structural connectivity to augment community structure in EEG functional connectivity

Katharina Glomb[1*], Emeline Mullier[1], Margherita Carboni[2,3], Maria Rubega[3], Giannarita Iannotti[3], Sebastien Tourbier[1], Martin Seeber[3], Serge Vulliemoz[2], Patric Hagmann[1]

1 Connectomics Lab, Department of Radiology, University Hospital of Lausanne and University of Lausanne, Lausanne (CHUV-UNIL), Vaud, Switzerland
2 EEG and Epilepsy, Neurology, University Hospitals of Geneva and University of Geneva, Geneva, Switzerland
3 Functional Brain Mapping Lab, Department of Fundamental Neurosciences, University of Geneva, Geneva, Switzerland
4 Department of Neurosciences, University of Padova, Padova, Italy

Abstract

Recently, EEG recording techniques (high-density EEG) as well as source analysis have improved markedly. Yet, analyzing whole-cortex EEG signals in source space is not standard, partly because EEG signals suffer from volume conduction, introducing spurious functional connections (statistical dependencies) between nearby sources. Genuine functional connectivity (FC) reflecting functional relationships is impossible to disentangle from spurious FC, impairing the applicability of network neuroscience to EEG. Here, we use information from white matter structural connectivity (SC) to attenuate the impact of volume conduction on EEG-FC. We confirm that FC (power envelope correlations) is predicted by the SC beyond the impact of Euclidean distance. We then smooth the EEG signal in the space spanned by graphs derived from SC. Thereby, FC between nearby, structurally connected brain regions is increased while FC between non-connected regions remains unchanged. We hypothesize that this results in an increase in genuine relative to spurious FC. We analyze changes in FC due to smoothing by assessing the resemblance between EEG- and fMRI-FC, and find that smoothing increases resemblance, both in terms of overall correlation and community structure. This suggests that information from the SC can indeed be used to attenuate the effect of volume conduction on EEG source signals.

Author summary

In this study, we combine high-density EEG recorded during resting state with white matter connectivity obtained from diffusion MRI and fiber tracking. We leverage the additional information contained in the structural connectome towards augmenting the source level EEG functional connectivity. In particular, it is known - and confirmed in this study - that the activity of brain regions that possess a direct anatomical connection is, on average, more strongly correlated than that of regions that have no such direct link. We use the structural connectome to define a graph and smooth the source reconstructed EEG signal in the space spanned by this graph. We compare the resulting “filtered” signal correlation matrices to those obtained from fMRI and find that such “graph filtering” improves the agreement between EEG and fMRI functional connectivity structure. Thus suggests that structural connectivity can be used to attenuate some of the limitations imposed by volume conduction.

Introduction

Understanding how flexible macroscopic functional architecture arises from the stable scaffold of anatomical white matter fiber tracts in the brain is a major field of inquiry in neuroscience. This has been investigated via the relationship between structural and functional connectivity (SC and FC, respectively) between brain regions in fMRI and MEG (Abdelnour, Dayan, Devinsky, Thesen, & Raj, 2018; Atasoy, Donnelly, & Pearson, 2016; Cabral et al., 2014; Damoiseaux & Greicius, 2009; Deco et al., 2013; Glomb, Ponce-Alvarez, Gilson, Ritter, & Deco, 2017; Goñi et al., 2014; Hagmann et al., 2008; Honey et al., 2009; Meier et al., 2016; Tewarie et al., 2019, 2014; Vincent et al., 2007). Concurring findings from these studies show that FC between regions of interest (ROIs)/sources located in the gray matter is in part shaped by anatomical connections of the SC, such that the strength of SC (fiber count, density) is predictive to some degree of the strength of FC (correlation, coherence, etc.) This finding has been shown to extend to EEG using data analytical (Chu et al., 2015; Wirsich et al., 2017) and modelling approaches (Bhattacharya, Coyle, & Maguire, 2011; de Haan, Mott, van Straaten, Scheltens, & Stam, 2012; Finger et al., 2016; Pons, Cantero, Atienza, & Garcia-Ojalvo, 2010; Ponten, Daffertshofer, Hillebrand, & Stam, 2010; van Dellen et al., 2013). However, the details of how SC and FC are related in EEG are unknown, and few tools are available.

In MEG and fMRI, whole-brain network neuroscience methods have yielded a multitude of important and interesting insights (see (Bassett & Sporns, 2017), for a review). In this approach, brain regions as defined by a functional or anatomical parcellations (Medaglia, Lynall, & Bassett, 2015) and are then used as nodes of a network. Edges between nodes are defined by functional, structural, or effective connectivity strengths. Characteristics of the whole network or of single nodes can then be extracted, interpreted, and compared across subjects, groups, or between experimental conditions. These methods are now being translated to EEG research (Babiloni et al., 2005; Chen, Ros, & Gruzelier, 2013; Chu et al., 2015; Coito, Michel, Vulliemoz, & Plomp, 2019; Finger et al., 2016; Siems, Pape, Hipp, & Siegel, 2016; Wirsich et al., 2017), but further validation and methodological developments, especially when it comes to resting state EEG, are necessary to make them more accessible for the community.

Compared to fMRI, M/EEG measure neural signals more directly (Buzsáki, Anastassiou, & Koch, 2012), and do so on a time scale (of milliseconds) much closer to that of neural events than fMRI (typically several 100 milliseconds to 2 seconds). Furthermore, even though electric currents generated by synchronized populations of neurons are responsible for both the magnetic fields measured by MEG and the electric fields measured by EEG, these signals actually predominantly reflect activity in different parts of the cortex, and should therefore be considered complementary. While the EEG signal is thought to originate mainly from the crowns of sulci (patches of cortex that are parallel to the skull), the MEG signal is thought to originate in the walls of sulci (patches of cortex that are perpendicular to the skull) (Srinivasan, Winter, & Nunez, 2006). Thus, EEG captures signals that neither MEG nor fMRI pick up.

On the other hand, the spatial resolution of EEG is low compared to that of fMRI or intracranial recordings; it is assumed that the EEG signal measured on the scalp summarizes synchronized activity occurring in patches of cortex as large as several cm^2 (Buzsáki et al., 2012), yielding a spatial resolution that is in general equal to that obtained with MEG (Schoffelen & Gross, 2009; Srinivasan, Winter, Ding, & Nunez, 2007). Furthermore, the macroscopic electrical signal is differentially filtered and attenuated by the different tissues of the head before it reaches the electrodes on the scalp, leading to a low signal to noise-ratio (SNR). This usually means that many (hundreds) of trials per subject are necessary in order to reach an acceptable SNR, making it difficult to apply to resting state data, where averaging is not generally possible.

Perhaps the main hurdle that prevents straightforward application of network neuroscience methods to EEG data is the fact that source localization is challenging. Additionally to the low spatial resolution and

SNR intrinsic to the EEG signal, the interaction of the electric field with the tissue is such that signals are distorted by volume conduction, unlike in MEG, because the tissues of the head are generally not magnetic (Malmivuo & Suihko, 2004; Srinivasan et al., 2007): An electrical potential induced by an electric current can be measured far away from the actual source of the current, and as a result, the activity time courses measured at different locations in the brain are correlated to a degree that depends on the Euclidean distance between these locations, creating “sham” functional connections. This effect of volume conduction obscures the genuine functional relationships between sources in the brain, which are also to some degree dependent on distance. *Inverse solutions* that are available for EEG are able to correct for some of these distortions by taking into account the conductivities of different kinds of tissues that are present in the head (Michel et al., 2004), especially if (like in the present study) individual head models derived from structural MRI scans are employed. Nevertheless, while source projection attenuates the problem, substantial signal leakage remains (Palva et al., 2018; Schoffelen & Gross, 2009).

In order to circumvent these problems, it has been suggested that zero-lag-statistical dependencies should be removed altogether from FC analysis since signal leakage is instantaneous, resulting in measures such as imaginary coherence (Nolte et al., 2004) and phase lag index (Stam, Nolte, & Daffertshofer, 2007), as well as approaches that orthogonalize the time series (Brookes, Woolrich, & Barnes, 2012; Colclough, Brookes, Smith, & Woolrich, 2015; Hipp, Hawellek, Corbetta, Siegel, & Engel, 2012; Wens et al., 2015). Contrary to this, it has been pointed out that zero-lag-statistical dependencies still carry meaningful information about ongoing activity (Pascual-Marqui et al., 2017; Tognoli & Kelso, 2009; Uhlhaas et al., 2009), and may therefore be particularly important for the resting state. Furthermore, the finding that some commonly used FC measures which remove zero-lag-dependencies, including imaginary part of coherence, phase lag index, and partial directed coherence, are highly correlated to FC measures which do not exclude these dependencies, like amplitude envelope correlation and coherence (Colclough et al., 2016), suggests that the former measures may not be fully effective at removing spurious correlations (Palva et al., 2018). Nevertheless, some recent studies have shown network structure partly concordant with fMRI resting state networks, and have added some directionality in network analysis (Coito, Michel, van Mierlo, Vulliemoz, & Plomp, 2016; Coito et al., 2019; Silfverhuth, Hintsala, Kortelainen, & Seppänen, 2012).

The results of the present study suggest that the relationship between SC and FC in EEG can be exploited in order to attenuate spurious statistical dependencies between source-level signals. We first replicate the previous finding (Chu et al., 2015; Finger et al., 2016; Siems et al., 2016; Wirsich et al., 2017) that SC partially shapes FC in EEG, beyond the impact of Euclidean distance induced by volume conduction. Subsequently, rather than applying signal orthogonalization or removing zero-lag-statistical interactions, we favor the approach of combining EEG with diffusion MRI (dMRI) and fMRI, modalities which have higher spatial resolution. On the one hand, we use additional information in the SC (obtained from dMRI and fiber tracking) to augment the EEG functional signal in a principled way by applying a low-pass filter in the space spanned by the SC-graph. On the other hand, we use an fMRI-FC acquired completely independently of the EEG dataset to show that by combining EEG and dMRI, we obtain EEG-FC which is more concordant with fMRI-FC, both overall and in terms of FC community structure. This suggests that EEG, fMRI, and dMRI provide complementary information about the anatomical and functional network structure of the brain. Our study shows new avenues to the application of network neuroscience and graph signal processing methods to EEG source level data, and demonstrates that these approaches are both useful and feasible.

Results

SC provides additional predictive power for EEG-FC

Our goal is to use the structural connectivity (SC) matrix to improve signal to noise-ratio (SNR) in source-level EEG time series by attenuating spurious statistical dependencies, and thus augment EEG functional connectivity (FC). Importantly, EEG signals recorded by 256 sensors on the scalp are source projected into the grey matter volume, allowing us to extract mean signals for each of 68 regions of interest (ROIs) defined by a standard cortical parcellation (Figure 1). EEG-FC is computed between these average time courses of all pairs of ROIs as correlations between low-frequency power modulations (see Methods) in three standard frequency bands: alpha (8-13 Hz), beta (13-30 Hz), and gamma (30-40 Hz). We first characterize the relationship between SC and EEG-FC averaged over all subjects (Chu et al., 2015; Finger et al., 2016; Wirsich et al., 2017). We fit a stepwise general linear model (GLM) in order to quantify how well the following measures predict the FC:

1) SC in the form of search information (Goñi et al., 2014), referred to as SC_{SI}, a measure that is derived from fiber counts and that is non-zero for all connections, yielding a connectivity matrix that is dense just like the FC matrix (Figure S8); the intuitive interpretation of search information is that it measures how "hidden" the shortest path between two ROIs is. Note that search information and fiber count are roughly *inversely* proportional.

2) Euclidean distance (ED) between ROI centers,

3) relative regional variance (i.e. the variance of each ROI time course, normalized such that the maximum variance in each subject equals 1) as an estimate of SNR,

4) ROI size (number of voxels in the parcellation).

The 3rd and 4th predictors are control variables for possible confounds. We analyze how well these variables can predict the FC in two different ways: On the one hand, we use each variable as the only predictor variable (plus intercept; blue bars in Figure 2; "single variable model"). On the other, we test their predictive power when they are entered progressively into a GLM that includes first order interaction terms (orange curves in Figure 2; "full model"). The latter case allows us to quantify the additional predictive power that each variable has given all other predictors. This is important because the predictors are not independent of each other; most prominently, there is a three-way-dependence between SC, Euclidean distance, and FC, such that both SC and FC decay with increasing Euclidean distance.

Figure 2A shows the results in terms of predictive power for the EEG-FCs and for comparison, for an fMRI-FC (average pairwise correlations over 88 subjects, see Methods for details; see SI Table 1 for detailed results of the GLM analysis). The correlation between the average EEG-FCs and the fMRI-FC is around 0.50 for all three bands (alpha, beta, gamma).

Figure 2A shows that ED is the strongest predictor in both EEG and fMRI. This is true both for the single variable models (greatest explained variance as indicated by blue bars) and the full model (as indicated by the fact that they are the variables that are entered first into the model). However, the variance explained by ED is much higher in EEG than in fMRI, namely 0.55 in EEG (alpha band; other bands similar, full list in Table S1) and 0.18 in fMRI. This is due to the effect of volume conduction which introduces spurious correlations dependent on ED in the case of EEG-FC.

A - Graph combining parcellation and structural connectivity

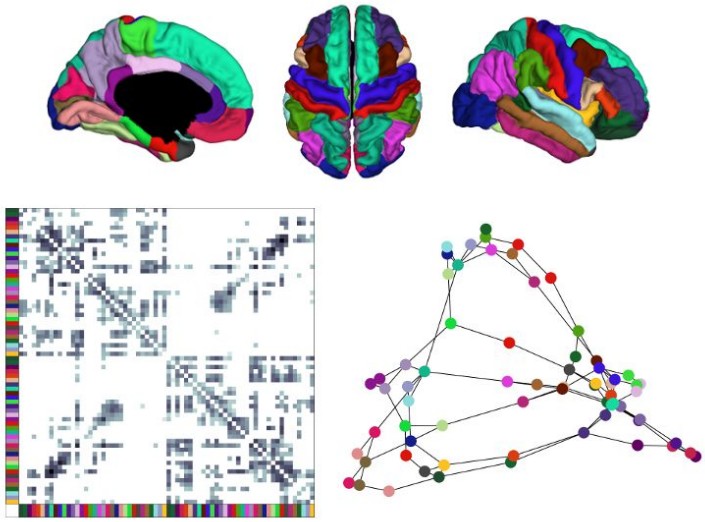

B - EEG signal in the graph domain

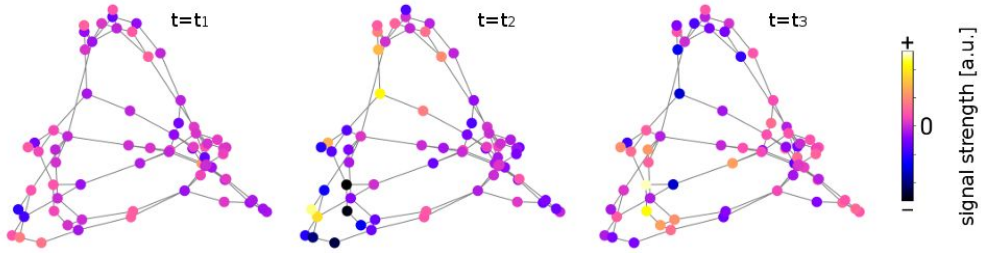

Figure 1: **A** - Brain regions are given by the Lausanne 2008 parcellation (top row). Diffusion MRI and fiber tracking reveal fiber bundles that exist between these regions, and are summarized in the structural connectivity matrix (bottom left; brain regions from above are color coded). The graph used for filtering is defined by nodes corresponding to the parcellation's brain regions (color coded) and edges corresponding to the fiber bundles in the SC matrix (bottom right; lengths of edges are approximately inversely proportional to the weight in the structural connectivity matrix). **B** - The graph defined by parcellation and SC does not change over time. EEG signals that do vary over time are conceptualized as activation strengths of the nodes of the graph. Signals are thought to propagate along the fiber bundles, i.e. the edges, to neighboring nodes.

When using SC_{SI} as the only predictor, we find that the dependency of FC on SC_{SI} is very similar in both modalities (r^2 of SC_{SI} alone 0.14 in both modalities). In both cases, SC_{SI} explains an additional 3-4% of the variance (SI Table 1). Note that the actual contribution of SC_{SI} is likely to be higher as SC strength is itself dependent on Euclidean distance (two regions that are close together are more likely to be connected by white matter tracts; furthermore, short tracts are more easily traced by fiber tracking algorithms, (Jones, 2010)). Indeed, due to this mutual dependence, the actual contribution of SC_{SI} cannot be estimated using this approach.

Furthermore, a significant positive interaction term between ED and SC_{SI} contributes to the prediction in both fMRI and EEG. The correlation between these two variables (ED and SC_{SI}) is 0.48, in line with previous findings (Wirsich et al., 2017). Since SC and SC_{SI} are negatively correlated (see Methods), this translates to two interpretations: ED has less of an impact on the FC between ROI pairs that have a strong SC-connection (high weight in the SC matrix); and the strength of the SC connection has less of an impact on the FC between ROI pairs that are far apart from each other (high ED).

The fact that in EEG, the relative regional variance (RRV) is the second-strongest predictor in terms of added explained variance indicates that noise due to source reconstruction and parcellation is unequally distributed across ROIs and contributes to biases in EEG-FC. This could be due to the fact that signals from deep sources are harder to pick up than those of superficial sources (Whittingstall, Stroink, Gates, Connolly, & Finley, 2003). However, the predictive power of this predictor on its own (blue bars) is very small.

A simple prediction from the hypothesis that FC is shaped by SC is that ROI pairs that are connected via white matter tracts should exhibit stronger FC than those that are not (Chu et al., 2015). A caveat is that both FC and SC have a genuine dependency on Euclidean distance - from an evolutionary standpoint, it makes sense for functionally related regions to be close together (Tomasi, Wang, & Volkow, 2013). In order to control for this, we compare subsamples of pairs of ROIs that are matched in their Euclidean distance distribution. Figure 2B shows that even in those matched subsamples, there is indeed a significant difference (Wilcoxon signed-rank test at alpha=0.05, Bonferroni-corrected for multiple comparisons) between structurally connected and unconnected ROI pairs.

A - Results of GLM analysis

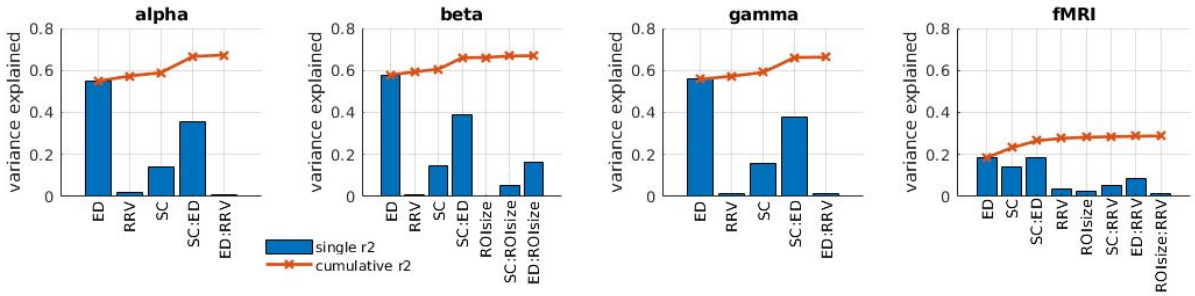

B - Comparison of FC with and without structural connections

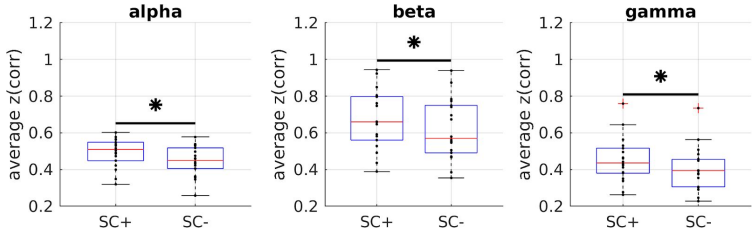

Figure 2: **A** - Stepwise general linear model results for EEG alpha, beta and gamma band, and for fMRI, using Euclidean distance (ED), relative regional variance (RRV), structural connectivity (SC; search information), and ROI size (number of voxels) as predictors. Only significant predictors are shown, in the order in which they were entered into the model (see Methods for details). Blue bars: variance explained when variables are used as the only predictor in separate “single variable” GLMs. Orange curves and crosses: Cumulative explained variance achieved when using all variables up to the variable corresponding to this data point (i.e. the variable in question and all variables to the left of the data point). **B** - Comparison between average EEG-FC values for pairs that are connected by SC (“SC+”) and those that are not (“SC-”). The samples that are compared are matched in their ED distribution to control for the fact that pairs that are connected tend to be closer together than those that are not. Stars mark significant differences according to the Wilcoxon signed-rank test at alpha=0.05 (Bonferroni-corrected for multiple comparisons).

Graph filtering increases resemblance between EEG-FC and fMRI-FC

Building on the finding that SC shapes EEG-FC beyond the impact of ED, we use the fact that the EEG data live on a graph defined by the SC (Figure 1). In the following, we perform spatial smoothing, or low-pass filtering, in graph space. This means that the nearest neighbors of an ROI are not defined in terms of their Euclidean (or geodesic) distances, but in terms of graph topology. The idea is that the activity in one node of the graph - an ROI - is smoothed by computing a weighted average of the ROI's activity and the activity of its nearest neighbors, i.e. nodes with which it is anatomically connected and from which it thus receives direct synaptic input:

$$\hat{x}_i(t) = x_i(t) + G \sum_{j=1}^{N} c_{ij} x_j(t)$$

Here, c_{ij} is the entry in the SC which corresponds to the pair of regions i and j, and G is the scalar "filter weight" which scales how much impact node i's neighbors j have on the activity of i. We expect that this will increase the effect shown in Figure 2B: Connected nodes' activity will become more similar and unconnected nodes' activity will become less similar. Since spurious correlations depend only on Euclidean distance, but not on the SC per se, this would correspond to an increase of genuine FC relative to spurious FC.

We filter the single epoch, source-level activity $x_i(t)$ of each ROI using the above formula and compute FC matrices from the filtered data $\hat{x}_i(t)$ as before. We use four different graphs (Figure 3, from left to right):

1. The SC (number of fibers) itself, averaged across subjects according to (Betzel, Griffa, Hagmann, & Mišić, 2019). This graph has a connection density of 25%.
2. A graph derived from Euclidean distances, setting connection weights with $exp(-k * ED)$, where the weight k just serves to scale the distribution. This is a dense graph and will be referred to as "ED full".
3. A graph derived from Euclidean distances, but exactly matching the SC in terms of existing and absent fibers. This means that the connections are the same as for SC 1, but the weights are set as in SC 2 instead of the fiber count. This graph will be referred to as "ED match".
4. A graph derived from Euclidean distances, but preserving the density of SCs 1 and 3. This means keeping the connections which correspond to the smallest EDs up to a threshold which leads to the same connection density as in SC1 (and SC 3). We include this graph because otherwise, if matrices 1 or 3 outperform matrix 2, this could just be due to the difference in connection density. This graph will be referred to as "ED dens".

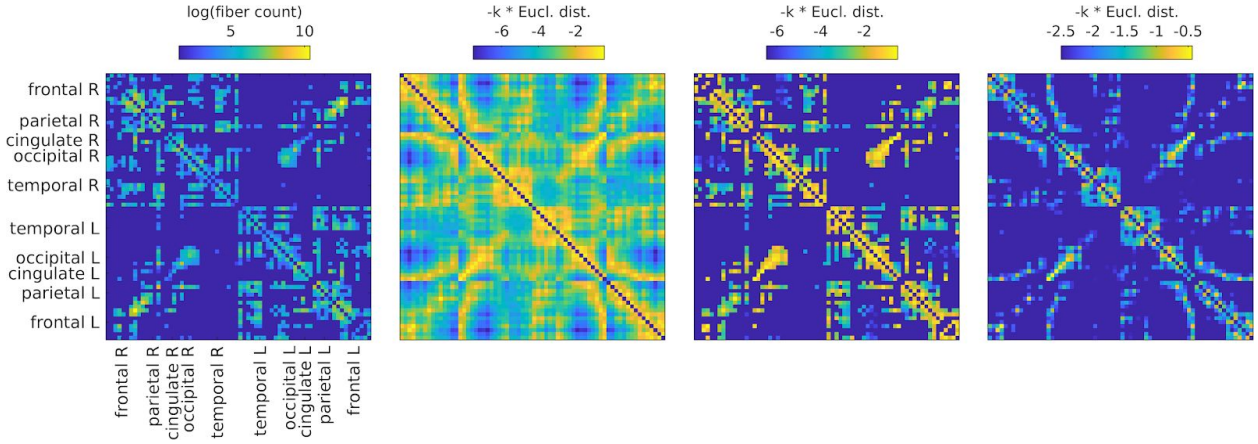

Figure 3: All SCs from which graphs for filtering are derived. From left to right. 1) SC derived from fiber tracking, averaged over subjects (log is used only for visualization purposes); 2) SC derived from Euclidean distances by using the distances as negative exponents; 3) SC derived from Euclidean distances (as 2), but masking the distances by using present connections as in 1); 4) SC derived from Euclidean distances (as 2), but keeping only shortest distances such that the density is the same as in the left and middle right panels.

A - Correlations between EEG- & fMRI-FC

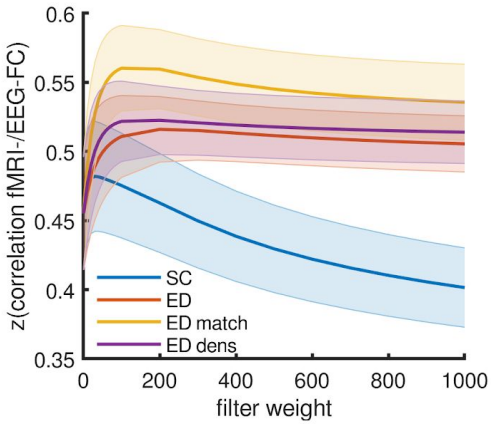

B - Boxplots of correlations

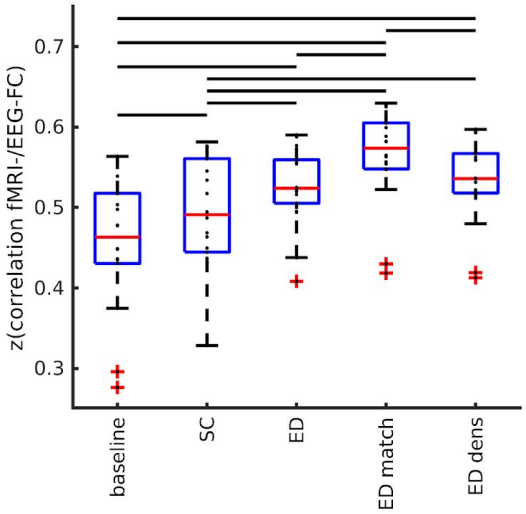

Figure 4: **A**:Fit (z-transformed correlation) between the EEG-FC (beta band) computed from time courses with different filter weights (G) and the fMRI-FC. The shaded regions mark the 95% confidence interval. **B**: Boxplots showing results of the Wilcoxon signed rank test comparing the maximum fits (shown in panel A) across versions of the SC as well as to the baseline correlation between unfiltered EEG-FC and fMRI-FC. Black bars mark significant differences. Red lines mark the median, each black dot marks the value for one subject.

After filtering, EEG-FCs are computed as for the unfiltered data. As expected, the filtered FCs become more similar to their respective SC_{SI}, and the difference in average correlation between structurally connected versus unconnected ROI pairs increases (see Figure S1).
To validate our results, we compare our EEG-FCs to fMRI-FC (obtained by averaging over 88 subjects, see Methods for details). We choose this approach because fMRI does not suffer from volume conduction, has a spatial resolution that is superior to that of EEG, and because recent studies have shown that the macroscopic network structure is, on a coarse level, similar between fMRI and EEG

despite the different temporal resolutions and the fact that the origin of the BOLD- and the EEG-signals are very different (Britz, Van De Ville, & Michel, 2010; Coito et al., 2019; Liu, Ganzetti, Wenderoth, & Mantini, 2018; Musso, Brinkmeyer, Mobascher, Warbrick, & Winterer, 2010). Furthermore, we compute envelope correlation-based EEG-FCs, capturing information similar to that of fMRI-correlation (Brookes et al., 2011; Hall, Robson, Morris, & Brookes, 2014). Therefore, we hypothesize that, if our filtering procedure indeed removes spurious correlations, the EEG-FCs resulting from the filtered time courses should be more similar to fMRI-FC than the original, unfiltered signals. We obtain a comparison for each filter weight G and each of the four graphs described above and shown in Figure 3.

Figure 4A shows that correlations between the two modalities increase as hypothesized (results shown for beta band, alpha and gamma similar [not shown]). The graph which reaches the highest maximum correlations between EEG- and fMRI-FC is the one in which Euclidean distance and SC are combined by masking the weights derived from Euclidean distances with the non-zero connections given by the SC ("ED match"; Wilcoxon signed rank test, $p<0.05$ Bonferroni corrected). The mean correlation increases from 0.42 to 0.51 at a filter weight of G=100, corresponding to a 23% increase (increase computed based on the Fisher z-transformed values as shown in Figures 4A and B: 0.46 and 0.56, respectively). Figure 5 shows the original EEG-FC (beta band) and the EEG-FC derived from filtered data with G=100. Importantly, we showed above that the correlation between SC and FC-fMRI is in fact slightly lower than that between SC and EEG-FC. This argument is even stronger for the "ED match"-matrix, which we again transformed to search information (see Methods) and found that its correlation to the fMRI-FC is -0.39, whereas that to the average EEG-FC (beta band) is -0.54. Hence, these observed improvements in correlation between EEG-FCs and fMRI-FC are not due to the fact that filtering increases the similarity between EEG-FC and SC/ED match.

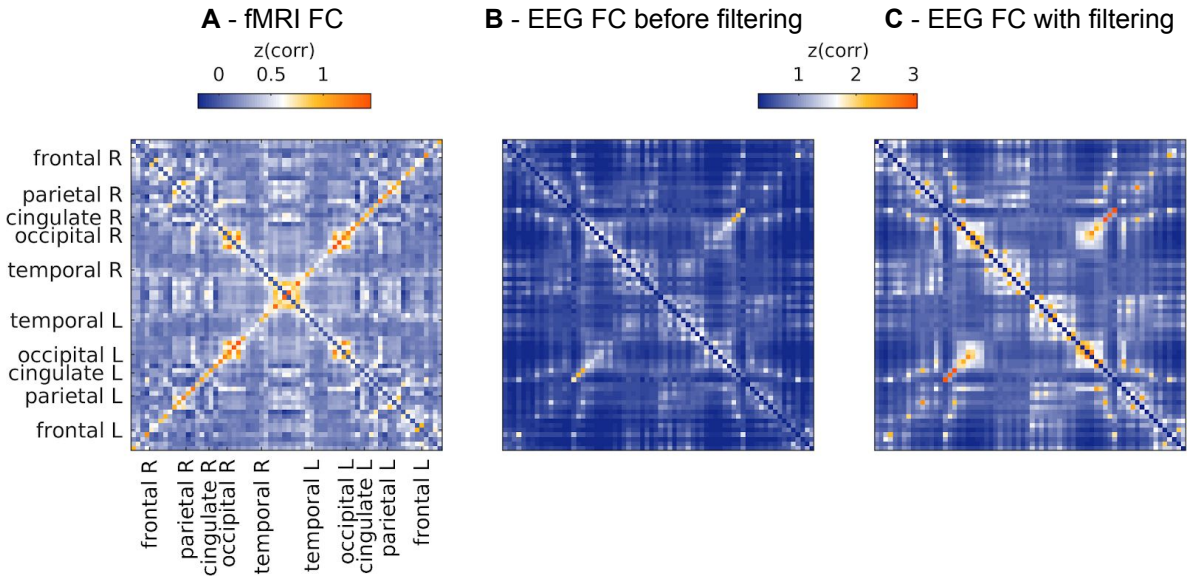

Figure 5: **A**: fMRI-FC. **B** and **C**: EEG-FCs (beta band) before (**B**) and after (**C**) graph filtering with "ED match" and G=100. All correlations are z-transformed.

Graph filtering increases resemblance between EEG- and fMRI-community structure

In the following, we explore the effect of graph filtering on the EEG-FC structure. To this end, we use FCs averaged over all subjects. First, we consider seed correlations. In order to make correlations comparable, we resample average FCs such that FC values are normally distributed around mean 0 and with a standard deviation of 1. Figure 6 shows the normalized correlations between two seed regions and all other ROIs in the parcellation (i.e. one row/column of the EEG-FC) before and after filtering with the

best SC identified above (“ED match”, G=100; beta band). We chose these regions because they exhibit the largest overall change in connection weights with other regions (all changes in Figure S2). In both cases, the correlations to the corresponding region on the other side of the brain are increased.
In general, the correlation structure of many regions changes considerably (Figure S2), but these changes are hard to interpret on a ROI by ROI basis. Therefore, to investigate this further, we extract the community structure of the average EEG-FCs before and after filtering by applying Louvain clustering as implemented in the Brain Connectivity Toolbox (Rubinov & Sporns, 2010). This algorithm maximizes the modularity of the network encoded in an adjacency matrix, in this case the FCs, by assigning each ROI to a community such that the intra-community FC is maximized while the inter-community FC is minimized. The final community structure depends to some degree on the initial random assignments, such that the outcome is not fixed. We take this stochasticity into account by repeating the clustering 200 times and estimating, for each pair of ROIs, the probability to be assigned to the same community (Figure 7, top row and bottom left). We apply the same procedure to the average fMRI-FC (Figure 7, bottom right). As the filter weight (G) increases, more values in these “community matrices” tend towards 0 or 1, indicating that the variability in clustering outcomes decreases. Interestingly, also the community assignments derived from the fMRI-FC show some variability, especially for certain frontal and temporal regions. Figure 8 shows one example of community assignments. The main difference between EEG and fMRI is that EEG community structure is dominated by the lobe architecture, whereas in fMRI, we see the robust clustering of frontal with middle temporal and posterior cingulate cortices, reminiscent of the default mode network (Laird et al., 2009), as well as the symmetry across hemispheres between temporal regions.

A - Changes in seed correlations of left rostral middle frontal regions

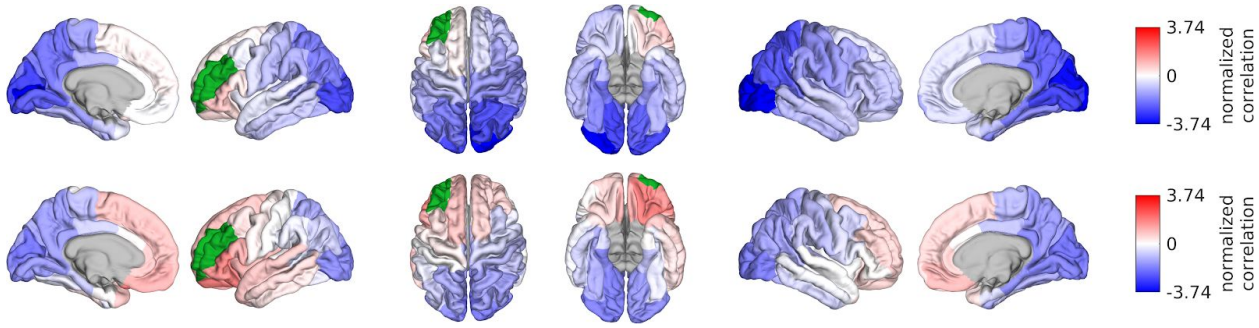

B - Changes in seed correlations of right superior parietal region

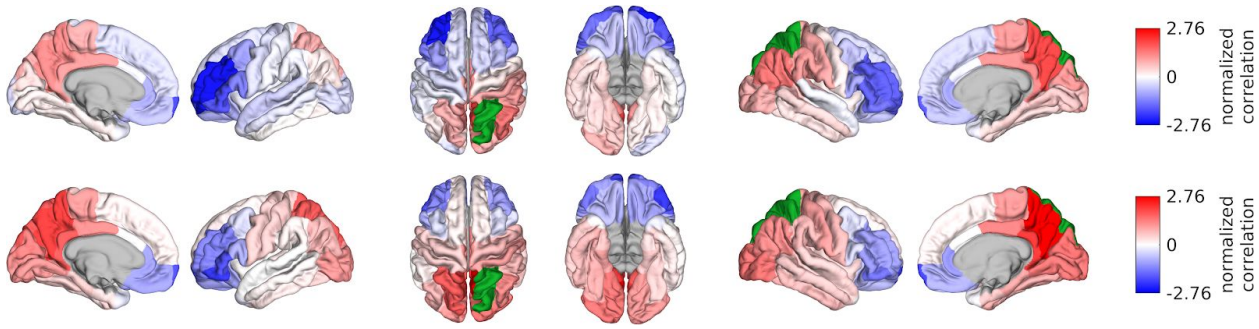

Figure 6: Surface renderings of FC before and after filtering. EEF-FC (beta band; correlation) values were resampled from a standard normal distribution in order to linearize them and make them comparable. **A**: Seed correlations of region left rostral middle frontal before (top panel) and after (bottom panel) graph filtering. **B**: Same as A, but for region right superior parietal.

We quantify the similarity between the community structures in EEG- and fMRI-FCs by taking the rank correlation between each row/column of the “community matrices” (examples for γ=1.1 in Figure 7). We compute this measure depending on two parameters: 1) the resolution parameter γ which controls the spatial resolution of the Louvain algorithm and thus the number of communities, and 2) the filter weight G. Figure 9A shows the averaged (over ROIs) similarity in community structure. There is a region where the average rank correlation is ~0.45, i.e. for filter weights between 200 and 1000 and $\gamma \geq 1.075$. At the same time, Figure 9B shows that with increasing γ, the number of communities also increases: The overall maximum in average rank correlation is 0.60 at γ=1.3 and G=800 (Figure S3), but at this point, we have 27 communities. Due to the coarseness of the parcellation used here, and according to the literature (Yeo et al., 2011), we seek to partition the cortex into as few communities as possible while also achieving a good agreement between the community structures of EEG- and fMRI-FCs. Choosing γ=1.1 (row indicated in Figures 9A and B), the number of communities is 5 and the agreement with the fMRI community structure is 0.45 (at G=200, 300, or 400, see Figure 9C). The same fit can be achieved at γ=1.125 and G=300, but at this point we have 6.5 communities on average. Similarly, without filtering, the correlation is 0.42, but the number of communities is 6. Thus, γ=1.1 and G=200, 300, or 400 represents the optimal tradeoff between number of communities and community agreement in comparison to other filter weights, including G=0.

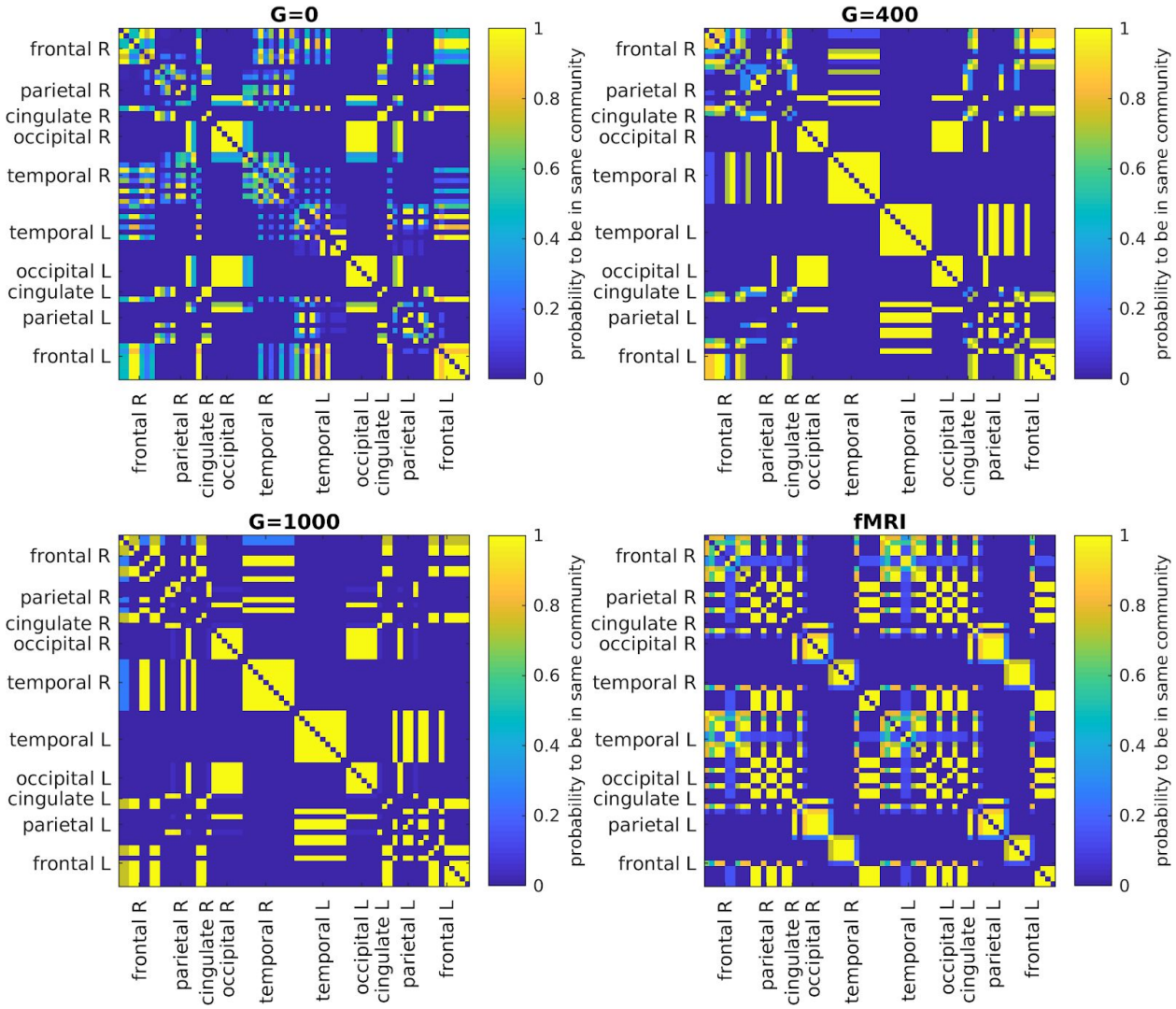

Figure 7: Results of Louvain clustering ("community matrices"). Each matrix shows, for each pair of ROIs, the fraction of repetitions of Louvain clustering (200 rounds, ɣ=1.1) which assigned both ROIs to the same community. ɣ=1.1 and G=400 (upper right matrix) are the parameter setting from a region of the parameter space where the agreement between EEG- and fMRI-community structures were found to be maximal (Figure 9; main text).

A Example EEG community structure before filtering

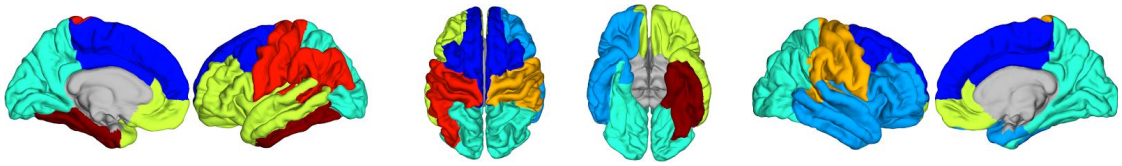

B Example EEG community structure after filtering (G=400)

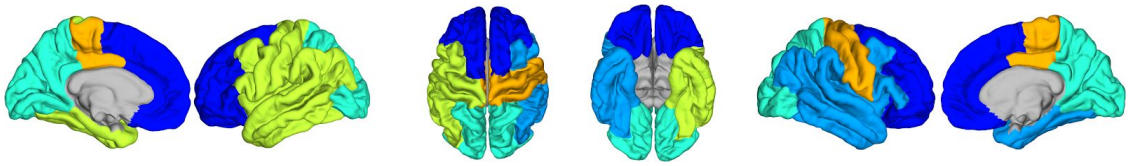

C Example fMRI community structure

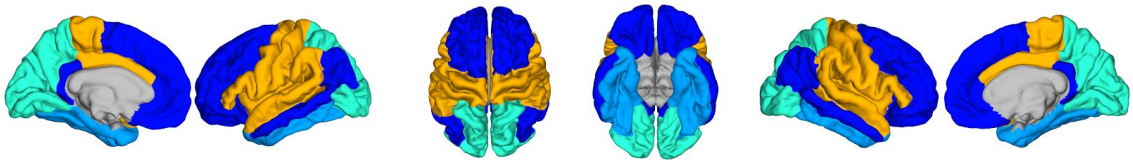

Figure 8: One result of Louvain clustering community assignments, γ=1.1. Graph filtering results, in this case, in a reduction of the number of communities from 7 (top panel, without filtering) to 5 (middle panel, G=400). The bottom panel shows one result for the fMRI-FC for comparison.

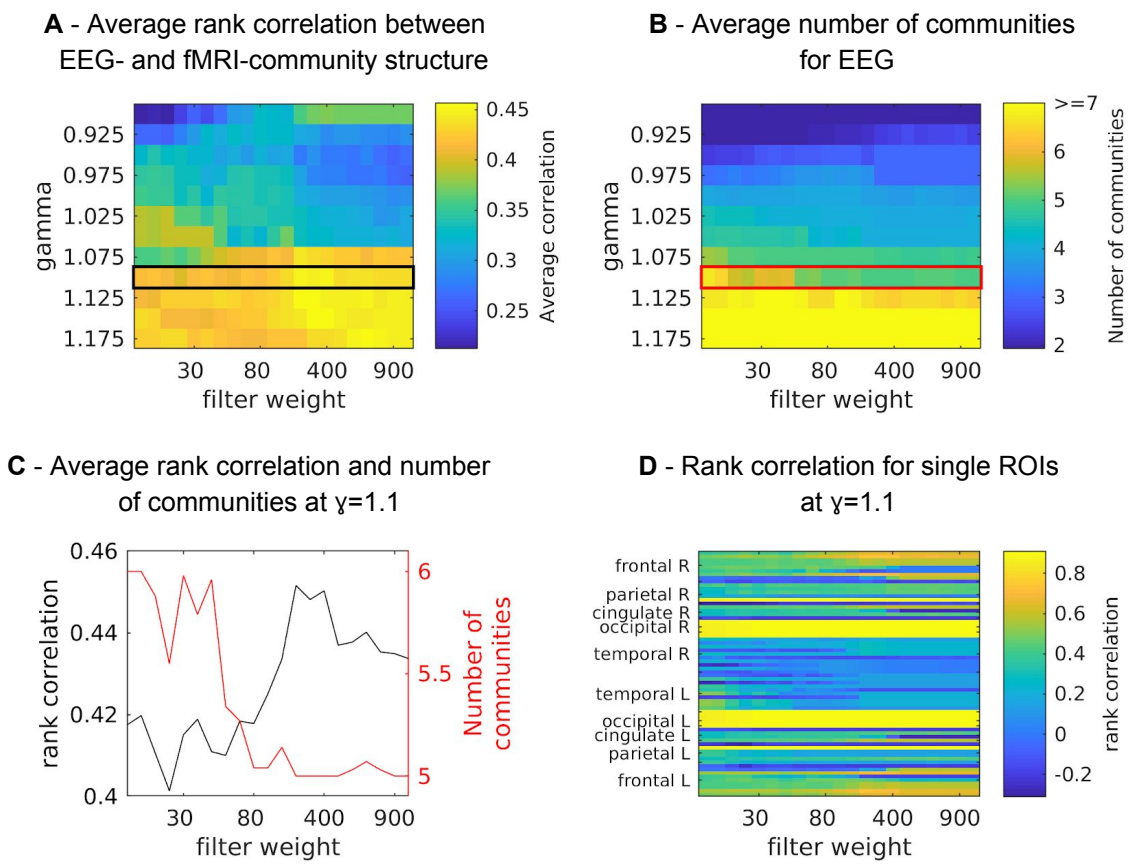

Figure 9: **A**: Agreement between community structure of EEG- and fMRI-FC as measured by average rank correlations between "community matrices" (Figure 7). The black box marks the γ which is shown in panel C. **B**: Average number of communities found by the Louvain clustering algorithm. The red box marks the γ which is shown in panel C. **C:** Rank correlations and number of communities for γ=1.1 (marked in the same colors in panels A and B). **D**: Rank correlations between rows/columns of "community matrices" (Figure 7) of EEG- and fMRI-FC, for γ=1.1 (marked with colored boxes in panels A and B).

In the following, we examine the behavior of different groups of ROIs in more detail for γ=1.1 and G=400. Remember that Figure 8 only provides an example partition and, as is evident in Figure 7, there is considerable variability in community co-assignments. By examining rows/columns of the community matrices in Figure 7, one can analyze the probability of a specific ROI to be co-assigned to the same community as all other ROIs. We call this the "community behavior" of this ROI. In Figures 10-12, we show this community behavior for selected ROIs in order to illustrate the changes in each of three major communities found by the Louvain algorithm: the frontal community, the somatosensory/motor network, and one of the two temporal communities; we do not show the occipital network as it is quite stable. Specifically, for one arbitrarily selected ROI that falls into each of these three communities, we plot, on the cortex, this ROI's row/column of the community matrices in Figure 7.

Figure 10 shows how the "community behavior" of an example frontal ROI (right lateral orbitofrontal ROI) differs between unfiltered and filtered EEG-FCs as well as fMRI-FC. The most conspicuous change that is introduced by the filtering is the establishment of a coherent frontal network which includes orbitofrontal regions, as in fMRI. This can be observed both in Figure 8 (blue network) as well as examining the changes in single ROIs displayed in Figure 9D.

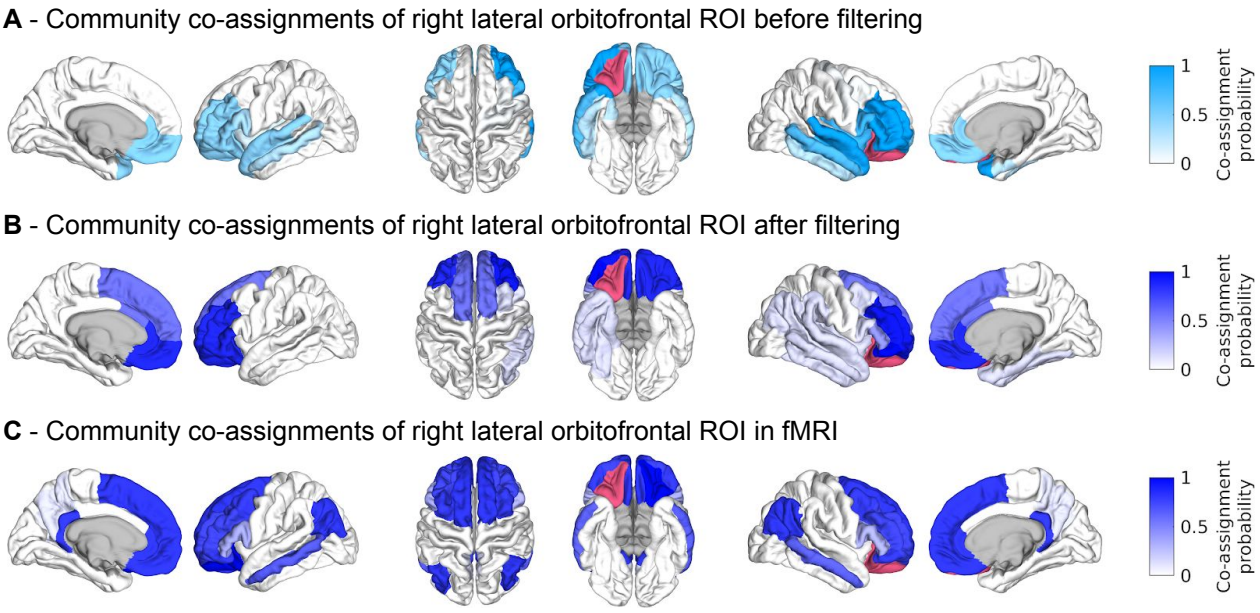

Figure 10: Community co-assignments of right lateral orbitofrontal ROI. **A**: Before filtering, there are two separate frontal networks (cf. Figure 8A), one more superior and one orbital, which also includes some temporal regions. **B**: After filtering, a single frontal network which is well-separated from other communities is established. **C**: Compared to fMRI, the FC to middle temporal, inferior parietal and posterior cingulate cortices is absent in EEG.

Figure 11 shows an example from the somatosensory/motor network (right paracentral lobule). This ROI shows a marked improvement in its agreement with fMRI. Namely, before filtering, this ROI is grouped with frontal regions (blue network in Figure 8). Afterwards, it becomes a member of the somatosensory/motor network (orange network in Figure 8), as is the case in fMRI. However, in contrast to fMRI, a symmetrical network is not established. This is due to the fact that the pre- and postcentral gyri are elongated and therefore, the Euclidean distances between ROI centers - which was used to establish the weights in the “ED match” graph - is quite high.

While the visual network is well-established even without any filtering (Figure 8, cyan network, and Figure 9D), temporal regions are mostly grouped due to their anatomical proximity. Figure 12 shows how the community behavior of an example temporal region (left fusiform ROI) changes due to filtering. Despite there being a qualitative improvement in that the region switches to a temporal network and decouples from visual regions, there are also many spurious co-assignments with other temporal regions which, in total, explain why this region shows no improvement due to filtering.

A - Community co-assignments of right paracentral lobule before filtering

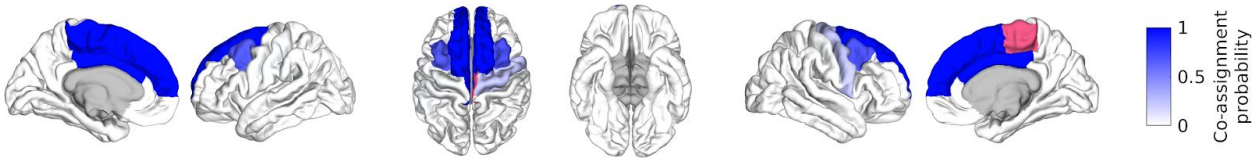

B - Community co-assignments of right paracentral lobule after filtering

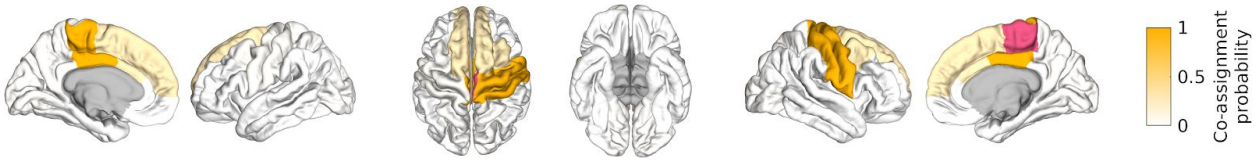

C - Community co-assignments of right paracentral lobule in fMRI

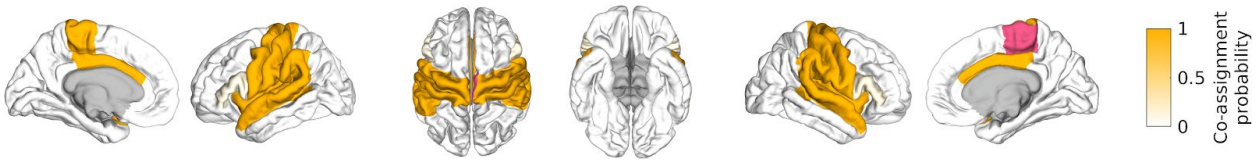

Figure 11: Community co-assignments of right paracentral lobule. **A**: Before filtering, this region is assigned to the same community as medial frontal regions. **B**: After filtering, these co-assignment probabilities are reduced and instead, the region is always grouped with pre- and postcentral gyri ipsilaterally as well as the contralateral paracentral lobule. **C**: In fMRI, this network includes the insula as well as some temporal regions and is symmetrical.

A - Community co-assignments of left fusiform ROI before filtering

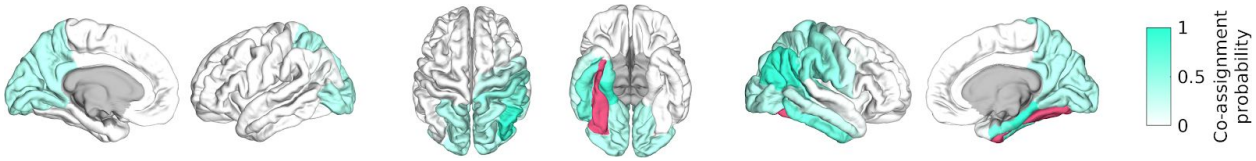

B - Community co-assignments of left fusiform ROI after filtering (G=400)

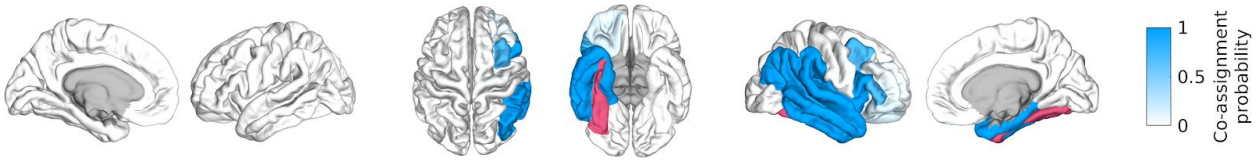

C - Community co-assignments of left fusiform ROI in fMRI

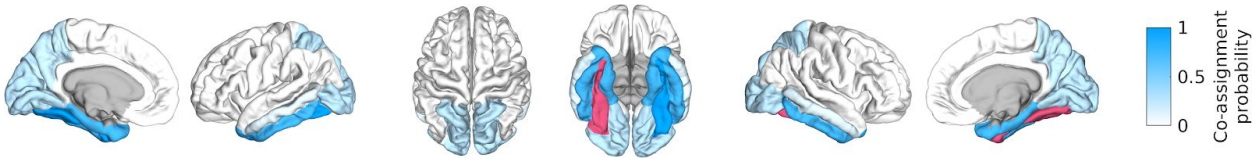

Figure 12: Community co-assignments of left fusiform ROI. **A**: Before filtering, the ROI belongs to the visual network (see Figure 8A), while **B**: after, as well as in **C**: fMRI, it belongs to a temporal network which is, however, not symmetric in the case of EEG.

Discussion

The main hurdle faced by researchers that want to apply network neuroscience methods to EEG source-level data is the strong impact of volume conduction which results in spurious FC determined by the Euclidean distance between sources. Without additional information (or a computational model), it is not possible to disentangle the effect of genuine dependence of FC on Euclidean distance from the spurious effect induced by volume conduction. In this study, we propose to use additional information present in the structural connectivity to selectively increase the FC between brain regions that are connected via white matter fibers and present evidence that this procedure attenuates spurious correlations introduced by volume conduction. Developing network neuroscience methodology for EEG functional networks is of wide interest because EEG is widely available, has excellent temporal resolution, and measures electrical signals generated in the brain directly.

We start by showing that the strength of FC between pairs of regions that are connected via SC is higher than between those pairs that are not. This difference is significant after the effect of Euclidean distance has been removed. This means that SC explains variance in the FC beyond the trivial relationship mediated by Euclidean distance. Additionally, there is a significant interaction between SC and Euclidean distance evident in the GLM analysis. Secondly, we find that using the SC graph to smooth functional EEG signals in nearest neighbor-graph space results in a higher agreement between fMRI- and EEG-FC structure. Comparing different nearest neighbor graphs, we find that the greatest improvement is achieved when we combine connectivity strengths derived from Euclidean distances and nearest neighbors determined by the presence or absence of white matter tracts ("ED match"). This is consistent with the SC-ED interaction found in the GLM. Lastly, we show that this improvement affects the large-scale network topography as probed by Louvain community structure. Also here, the agreement between the community structure found in fMRI-FC and that found in EEG-FC is increased due to filtering.

SC is outperformed by graphs (partially) derived from Euclidean distance

The result that a combination of SC and Euclidean distance performs best was – though consistent with the strong interaction term between Euclidean distance and SC in the GLM – contrary to our initial expectation that SC (fiber counts) would give the largest improvement. We propose three explanations for this observation.

1. The SC matrix is not a perfect description of the white matter fiber tracts in the brain. Most importantly, some interhemispheric as well as long fibers running in frontal to occipital direction are missing, such that some aspects of the FC cannot be captured by the filtering procedure even though in reality, they are directly supported by the SC. We illustrate this explicitly for the temporal lobes (Figure 12). Furthermore the true relationship between number of fiber tracking streamlines and effective coupling strength between cortical regions is unknown.
2. Our rationale for using the SC to modify FC is that smoothing in graph space would remove some of the effect of volume conduction by reinforcing signal similarity between cortical regions known to interact directly. However, when using the fiber counts alone, the FC between areas that are connected in the SC is strengthened by the filtering procedure regardless of their Euclidean distance. This means that the FC between remote areas, which is expected to be less affected by volume conduction, is also modified. We could suppose that the FC between remote areas is already less biased by volume conduction (estimated within the precision afforded by the limited spatial resolution of the EEG signal), and that additional information from the SC is not able to improve this estimate. The possible explanation why combining SC topology with ED weighting is optimal might be because it maximally "corrects" the signal according to

underlying structural organization where volume conduction is maximal, namely in the close surrounding of an area, while at large distance, where volume conduction is much lower, the signal is hardly corrected. 3. Using the (dense) connectivity matrix derived from Euclidean distances alone also resulted in significant improvement, in fact outperforming the SC. This amounts to simple spatial smoothing, further blurring a signal that is already recorded with low spatial precision. To us, this suggests that the parcellation used here – the standard FreeSurfer parcellation – is not optimal for EEG. The ROIs of this parcellation are mostly anatomically defined, not taking into account the nature of the EEG signal: Regions are highly unequal in size, resulting in a wide range of numbers of dipoles being averaged to obtain the ROI time courses. Furthermore, ROIs are in many cases elongated, while for EEG, more spherical regions (as far as this would be anatomically/functionally plausible) would be preferable. Finally, the appropriate number of ROIs is a matter of debate, as a simple correspondence between the number of ROIs and the number electrodes is not applicable (Farahibozorg, Henson, & Hauk, 2018).

Euclidean distance and fiber count differentially affect FC in different communities

Our community analysis, using Louvain clustering, revealed that EEG functional networks are differentially affected by our filtering procedure (using “ED match”). For frontal regions, robust improvements are observed, yielding a network that resembles that found in fMRI, apart from missing functional connections that would constitute the hallmarks of the default mode network, i.e. long-range connections between frontal regions and the middle temporal, inferior parietal, and posterior cingulate cortices. However, note that with this coarse anatomical - not functional - parcellation, even the fMRI community structure does not clearly resolve the DMN, which is mixed with the frontoparietal network. This indicates that for this network, “ED match” is a good choice.

For temporal regions, fMRI shows a distinct structure which is not reproduced by EEG either with or without filtering. The main difference is that there is no FC across hemispheres between temporal regions. This shows a limitation of our approach (see below for more discussion on limitations), because even in the SC, there are very few, if any, white matter fiber tracts between the temporal lobes. This is because these fibers are very long and pass through the corpus callosum, making them hard to track. Beyond that, in fMRI, superior, middle, and inferior temporal gyri belong to different networks (somatosensory/motor/auditory, default mode/frontoparietal, limbic/visual, respectively – the resolution of this parcellation is too coarse to resolve these systems properly), while in EEG, the anatomical architecture of the lobes determines the partition into communities. This is a shortcoming which could potentially be improved by using a more EEG-appropriate parcellation.

Finally, for parietal regions typically belonging to a prominent somatosensory/motor network, improvements are achieved using “ED dens”, however, the typical symmetric network including pre- and postcentral gyri is not established. When using the SC graph for the smoothing procedure, this network is robustly expressed in a certain area of the parameter space (Figures S4 and S5), however, the overall correspondence between EEG- and fMRI-FCs and community structures is much lower at this point (average rank correlation: 0.22). Therefore, for this network, SC is the better choice even though overall, SC is outperformed by all ED-based graphs.

These observations are in line with recent findings that show that the alignment between SC and FC, i.e. the degree to which FC is shaped by SC, differs across regions (Preti & Van De Ville, 2019), with sensory regions - i.e. the visual and somatosensory/motor cortices - are more strongly aligned with the SC than higher cognitive areas.

Limitations

We have already mentioned two limitations of our methodology. First, the SC has obvious shortcomings like the absence of many interhemispheric fibers and the underestimation of long fibers, which are hard to track (Jeurissen, Descoteaux, Mori, & Leemans, 2019; Jones, 2010). Second, the parcellation used here was developed for fMRI and is largely based on anatomical considerations. Another limitation is that we used envelope-based correlations which are known to be strongly influenced by volume conduction. We opted for this measure because it is widely used (Cabral et al., 2014; Hipp et al., 2012; O'Neill, Barratt, Hunt, Tewarie, & Brookes, 2015) and captures predominantly slow power modulations, which is closer to what the BOLD signal would capture. However, we did conduct our analyses using coherence and imaginary part of coherence (Figures S6 and S7) and found no major differences. This is in line with research that shows that FCs obtained with these measures show correlations of ~0.9 and above in MEG (Colclough et al., 2016), and with the finding that even measures which are theoretically immune to volume conduction because they remove contributions from zero-phase lag correlations/coherence, are in practice still heavily influenced by these effects (Palva et al., 2018). On the conceptual level, it is unclear how much EEG-FC should resemble fMRI-FC, since BOLD and the EEG signal are related in a way that is not straightforward. At the same time, recent studies show that RSNs are quite similar across these modalities and therefore, on this level of resolution and detail, we should expect a good agreement between the FC matrices (Coito et al., 2019; Liu et al., 2018).

Conclusions and future work

Taken together, we add to the thus far sparse knowledge on how SC and FC are related in EEG source space. Developing these methods is crucial for taking full advantage of the immense richness of the EEG signal in the temporal and frequency domain, and combining EEG with other modalities like MEG and fMRI. We have limited our analysis to the grand-average FC, but our method could be used to improve SNR on the single trial level, potentially easing statistical analysis of task-EEG in source space. One important conclusion from our results is that EEG-specific parcellation schemes are necessary to guarantee that we take full advantage of the richness of the EEG signal. Furthermore, our results confirm that it is feasible and sensible to use dynamical models that assume functional activity to spread through white matter fibers in EEG (Bhattacharya et al., 2011; de Haan et al., 2012; Finger et al., 2016; Pons et al., 2010; Ponten et al., 2010; van Dellen et al., 2013). On the data analysis side, this study provides a justification and an avenue to applying more sophisticated methods like graph signal processing (Shuman, Narang, Frossard, Ortega, & Vandergheynst, 2012).

Methods

EEG Data and source projection

Data were recorded from 21 healthy controls as part of an epilepsy study at the EEG and Epilepsy Unit, University Hospital of Geneva. This study was approved by the local ethics committee. 3 subjects were excluded due to too many movement artifacts, leaving 18 for analysis. Since subjects were age-matched to patients (not analyzed here), 6 subjects aged less than 18 years were included (age range: 8 to 54 years, median: 29.5). Since we could not find any qualitative differences when excluding these subjects, we proceeded with using all 18 available datasets.

Resting state EEG was collected with the Geodesic Sensor Net with 256 electrodes (Electrical Geodesic, Inc., Eugene, USA) during resting state. Electrodes on cheeks and neck were excluded, leaving 204 electrodes for analysis. Data were downsampled to 1 kHz and artifacts were removed by Infomax-based ICA prior to source projection. Remaining artifacts were marked manually and visually and markers were later used to extract artifact-free intervals of varying length and number per subject (Table S2). Inverse solutions were computed using LAURA with LSMAC as implemented in CARTOOL (Brunet, Murray, & Michel, 2011), employing individual head models that were extracted from T1-weighted images (acquired as magnetization prepared rapid-gradient echo MPRAGE volumes with a Siemens TrioTim 3T MRI scanner and a tfl3d1ns pulse sequence with flip angle = 9°; echo time = 2.66ms, repetition time = 1.51s, inversion time = 0.9, voxel size = $1\times1\times1mm^3$ head first supine) obtained from the same subjects in order to create the forward model. Segmentation and ROI extraction (i.e., parcellation) was performed using Connectome mapper 3 (Tourbier, Aleman-Gomez, Griffa, Bach Cuadra, & Hagmann, 2019). Gray and white matter were segmented from the MPRAGE volume using Freesurfer with the Lausanne 2008 multiscale parcellation (Hagmann et al., 2008), whose first scale corresponds to the Desikan atlas (Desikan et al., 2006).

Data were source projected to ~5000 dipole locations equally spaced on a 3D-grid, where the grey matter volume extracted from the same images served as a constraint for the dipole locations. ROI-time courses were obtained by performing SVD on the time courses of all solution points within an ROI and projecting onto the main direction of variance (Rubega et al., 2019).

MRI data

88 healthy control subjects (mean age 29.7 years, minimum 18.5, maximum 59.2 years; 34 females) were scanned in a 3-Tesla MRI scanner (Trio, Siemens Medical, Germany) using a 32-channel head-coil. Informed written consent in accordance with institutional guidelines (protocol approved by the Ethics Committee of Clinical Research of the Faculty of Biology and Medicine, University of Lausanne, Switzerland, #82/14, #382/11, #26.4.2005) was obtained for all subjects.A large subset (70 out of 88 subjects) of the structural and functional connectivity matrices obtained from this data are available on Zenodo (Griffa, Alemán-Gómez, & Hagmann, 2019), where the processing pipelines are described in detail. Briefly, for diffusion imaging, a DSI sequence (128 diffusion-weighted volumes and a single b0 volume, maximum b-value 8,000 s/mm^2, 2.2x2.2x3.0 mm voxel size) was applied. For resting state fMRI, a gradient echo EPI sequence sensitive to BOLD contrast (3.3-mm in-plane resolution and slice thickness with a 0.3-mm gap, TR 1,920 ms, resulting in 280 images per participant) was applied. A magnetization-prepared rapid acquisition gradient echo (MPRAGE) sequence sensitive to white/gray matter contrast (1-mm in-plane resolution, 1.2-mm slice thickness) was also acquired. ROI extraction (i.e., parcellation) was performed using the Connectome mapper (Daducci et al., 2012). Gray and white matter were segmented from the MPRAGE volume using Freesurfer with the Lausanne 2008 multiscale parcellation (Hagmann et al., 2008), whose first scale corresponds to the Desikan atlas (Desikan et al.,

2006). DSI data were reconstructed following the protocol described in (Van J. Wedeen, Hagmann, Tseng, Reese, & Weisskoff, 2005).
Structural connectivity matrices were estimated for individual participants using deterministic streamline tractography on reconstructed DSI data, initiating 32 streamline propagations per diffusion direction, per white matter voxel (V. J. Wedeen et al., 2008).
FMRI volumes were corrected for physiological variables, including regression of white matter, cerebrospinal fluid, as well as motion (three translations and three rotations, estimated by rigid body co-registration). Time courses of voxels falling into each ROI were average and FC was computed as correlations between these ROI time courses.

Functional connectivity measures for EEG
For our main analysis, we used power envelope correlations to measure functional connectivity in alpha (8-13 Hz), beta (13-30 Hz), and gamma (30-40 Hz) bands. All data analysis was performed in Matlab 2017a (MathWorks, Natick, USA). We extracted artifact-free intervals from the resting state time courses by using the artifact markers mentioned above, admitting only intervals of at least 19s duration in order to guarantee a reliable estimation of slow envelope modulations (see below). Prior to extracting the FCs, for each artifact-free interval, the data were downsampled to 250 Hz in order to avoid numerical errors which can be induced if the band of interest is much lower than the sampling rate.
Envelope correlations were computed as in (Cabral et al., 2014): after zero-phase band-pass filtering (eegfilt from EEGLAB software package) the EEG single trial time series in the respective bands, envelopes were extracted using the Hilbert transform. Envelopes were again low-pass filtered at 0.5 Hz, capturing ultraslow modulations in the respective bands. This measure was chosen to be as closely related as possible to fMRI-FC (Pearson correlation between BOLD time courses).
As a comparison (see Discussion), we computed the EEG-/fMRI-FC-correlations also using FCs obtained with coherence and imaginary part of coherence (icoherence, (Nolte et al., 2004). This part of the analysis was performed using functions implemented in the Brainstorm toolbox (Tadel, Baillet, Mosher, Pantazis, & Leahy, 2011), which is documented and freely available for download online under the GNU general public license (http://neuroimage.usc.edu/brainstorm). Brainstorm estimates (i)coherence in a minimum number of 5 windows which overlap by 50%. At a sampling rate of 250 Hz, this results in a minimum required signal length of ~3s. Thus, artifact-free intervals were segmented into epochs of ~3s. Since we found that these measures were more susceptible to noise introduced by remaining artifacts than envelope correlations, we further rejected epochs which, at any point, deviated from the mean by more than 6 standard deviations. See Table S2 for the number of epochs that was used for each subject.

Average SCs
All data analysis was performed in Matlab 2017a (MathWorks, Natick, USA). We used the method introduced in (Betzel et al., 2019), to obtain an unbiased average SC (average number of fibers). In brief, this method takes into account the fact that interhemispheric connections are less reliable than intrahemispheric ones. Using a single recurrence-based threshold on the average SC (i.e. setting all connections that are present in less than a certain percentage of subjects to 0) results in an underestimated interhemispheric connection density compared to single subjects. This method preserves both intra- and interhemispheric connection density found in single subjects by applying separate thresholds. Additionally, we require a recurrence of at least 30%. The resulting connection density in our SC is 25%.

Search information

All data analysis was performed in Matlab 2017a (MathWorks, Natick, USA). In order to correlate FC and SC matrices, we have to overcome the problem that FCs are dense (Pearson correlation of time courses can be computed for all pairs of ROIs), while fiber tracts only exist between a subset of ROI pairs. Here, we use search information as defined in (Goñi et al., 2014) to derive a dense matrix SC_{SI} from the SC. A path $\pi_{s\to t}$ is a sequence of edges (non-zero entries in the SC) leading from node s to node t. The search information $S(\pi_{s\to t})$ is then computed as

$$S(\pi_{s\to t}) = -log_2(P_{(\pi_{s\to t})})$$

where

$$P_{(\pi_{s\to t})} = \Pi_{i\in\Omega^*_{s\to t}}(\pi^{(1)}{}_{i\to t}/w_i)$$

$P_{(\pi_{s\to t})}$ is the probability that a signal travelling from node s to node t will take the shortest path $\pi_{s\to t}$. $\Omega^*{}_{s\to t}$ is the sequence of nodes on the shortest path, $\pi^{(1)}{}_{i\to t}$ is the first element (edge) on the path from node i to node t, and w_i is the weight of this edge. The intuition is that if there exist many such sequences between two given nodes s and t, the shortest path is "hidden" and more "information" is needed to find it. Figure S8 shows this matrix.

General linear model

We use Matlab's function stepwiseglm() to compute coefficients and p-values for a general linear model (GLM) that computes FC from four predictors:

1. search information derived from SC, as detailed above
2. Euclidean distance
3. relative regional variance (RRV)
4. ROI size

RRV serves as a proxy for signal to noise ratio. First, we compute for each ROI and each subject the average (over intervals) variance of this ROI's time courses. The variances are then scaled such that the maximum (over ROIs) variance is 1 and averaged over subjects.

Matlab's stepwiseglm() finds the order of predictor variables in terms of their deviances, i.e. twice the difference between the log-likelihood of that model and the full model (using all possible predictors, i.e. 4 main effects and 6 interaction terms). A variable is added into the model if the difference between deviances obtained by adding it is significant (χ^2 test). Removal of a term is also possible; this can occur if predictors are linearly dependent. Any non-significant predictors are not included. Interactions are only included if the main effects are significant. For comparison, we fit single-variable GLMs that use only the intercept and one predictor variable at a time (see Figure 2A).

Smoothing in graph space

Figure 1 illustrates our filtering approach. We performed spatial low-pass filtering, or smoothing, using the space defined by different versions of the structural connectivity graph. Each node of this weighted and undirected graph is one region of interest defined by the Lausanne2008 parcellation scheme (Hagmann et al., 2008), yielding 68 nodes. The edges of the graph are defined by the density of white matter tracts discovered between these ROIs via dMRI. Smoothing of node i's signal at time t, $x_i(t)$, is then performed using the nearest neighbors of node i, i.e. all nodes $j \neq i$ which have a direct connection to i according to the connectivity matrix C with entries c_{ij}:

$$\hat{x}_i(t) = x_i(t) + G \sum_{j=1}^{N} c_{ij} x_j(t)$$

$\hat{x}_i(t)$ is the resulting filtered signal. G is a scalar parameter $0 \leq G \leq 1000$ which tunes the impact of the neighbors' signal. The filtering procedure was implemented using Matlab 2017a.

Analysis of community/modular structure of FC matrices

We used the Louvain community detection algorithm implemented in the Brain Connectivity toolbox (Rubinov & Sporns, 2010) to evaluate the community structure present in the FC matrices. This algorithm takes the FC (adjacency) matrix and assigns each ROI to a community. The function takes one parameter, γ, which controls the spatial resolution and thus, indirectly, the number of communities that are detected, with higher values of γ leading to more and smaller communities. We varied γ in a range of $0.9 \leq \gamma \leq 1.3$, resulting in a minimum of 2 and a maximum of 35 communities (Figure S3).

Since the community structure depends to some degree on the initial conditions (randomly assigned module memberships of ROIs), we repeated the procedure 200 times. Instead of opting for a "hard assignment" approach, we took into account the uncertainty of the cluster structures. For each round of clustering, we determined for each pair of ROIs whether they were assigned to the same community. This resulted in a "community matrix" which can be interpreted as indicating the probability of a pair of ROIs to belong to the same community. Thus, each row/column of one of these matrices describes the "community profile" of a given ROI. In order to compare the community structures of EEG- vs fMRI-FCs, we compute the rank correlations between the community profiles (row/column of community matrix) of each ROI.

Acknowledgements

This work was supported by Swiss National Science Foundation Sinergia grant no. 170873 and grant no. 169198 (to S. Vulliemoz).

We thank Mina Jamshidi Idaji for her valuable comments on this project.

References

Abdelnour, F., Dayan, M., Devinsky, O., Thesen, T., & Raj, A. (2018). Functional brain connectivity is predictable from anatomic network's Laplacian eigen-structure. *NeuroImage*, *172*, 728–739.

Atasoy, S., Donnelly, I., & Pearson, J. (2016). Human brain networks function in connectome-specific harmonic waves. *Nature Communications*, *7*, 10340.

Babiloni, F., Cincotti, F., Babiloni, C., Carducci, F., Mattia, D., Astolfi, L., … He, B. (2005). Estimation of the cortical functional connectivity with the multimodal integration of high-resolution EEG and fMRI data by directed transfer function. *NeuroImage*, *24*(1), 118–131.

Bassett, D. S., & Sporns, O. (2017). Network neuroscience. *Nature Neuroscience*, *20*(3), 353–364.

Betzel, R. F., Griffa, A., Hagmann, P., & Mišić, B. (2019). Distance-dependent consensus thresholds for generating group-representative structural brain networks. *Network Neuroscience (Cambridge, Mass.)*, *3*(2), 475–496.

Bhattacharya, B. S., Coyle, D., & Maguire, L. P. (2011). Alpha and Theta Rhythm Abnormality in Alzheimer's Disease: A Study Using a Computational Model. *From Brains to Systems*,

57–73. Springer New York.
Britz, J., Van De Ville, D., & Michel, C. M. (2010). BOLD correlates of EEG topography reveal rapid resting-state network dynamics. *NeuroImage*, *52*(4), 1162–1170.
Brookes, M. J., Hale, J. R., Zumer, J. M., Stevenson, C. M., Francis, S. T., Barnes, G. R., … Nagarajan, S. S. (2011). Measuring functional connectivity using MEG: methodology and comparison with fcMRI. *NeuroImage*, *56*(3), 1082–1104.
Brookes, M. J., Woolrich, M. W., & Barnes, G. R. (2012). Measuring functional connectivity in MEG: a multivariate approach insensitive to linear source leakage. *NeuroImage*, *63*(2), 910–920.
Brunet, D., Murray, M. M., & Michel, C. M. (2011). Spatiotemporal analysis of multichannel EEG: CARTOOL. *Computational Intelligence and Neuroscience*, *2011*, 813870.
Buzsáki, G., Anastassiou, C. A., & Koch, C. (2012). The origin of extracellular fields and currents--EEG, ECoG, LFP and spikes. *Nature Reviews. Neuroscience*, *13*(6), 407–420.
Cabral, J., Luckhoo, H., Woolrich, M., Joensson, M., Mohseni, H., Baker, A., … Deco, G. (2014). Exploring mechanisms of spontaneous functional connectivity in MEG: how delayed network interactions lead to structured amplitude envelopes of band-pass filtered oscillations. *NeuroImage*, *90*, 423–435.
Chen, J.-L., Ros, T., & Gruzelier, J. H. (2013). Dynamic changes of ICA-derived EEG functional connectivity in the resting state. *Human Brain Mapping*, *34*(4), 852–868.
Chu, C. J., Tanaka, N., Diaz, J., Edlow, B. L., Wu, O., Hämäläinen, M., … Kramer, M. A. (2015). EEG functional connectivity is partially predicted by underlying white matter connectivity. *NeuroImage*, *108*, 23–33.
Coito, A., Michel, C. M., van Mierlo, P., Vulliemoz, S., & Plomp, G. (2016). Directed Functional Brain Connectivity Based on EEG Source Imaging: Methodology and Application to Temporal Lobe Epilepsy. *IEEE Transactions on Bio-Medical Engineering*, *63*(12), 2619–2628.
Coito, A., Michel, C. M., Vulliemoz, S., & Plomp, G. (2019). Directed functional connections underlying spontaneous brain activity. *Human Brain Mapping*, *40*(3), 879–888.
Colclough, G. L., Brookes, M. J., Smith, S. M., & Woolrich, M. W. (2015). A symmetric multivariate leakage correction for MEG connectomes. *NeuroImage*, *117*, 439–448.
Colclough, G. L., Woolrich, M. W., Tewarie, P. K., Brookes, M. J., Quinn, A. J., & Smith, S. M. (2016). How reliable are MEG resting-state connectivity metrics? *NeuroImage*, *138*, 284–293.
Daducci, A., Gerhard, S., Griffa, A., Lemkaddem, A., Cammoun, L., Gigandet, X., … Thiran, J.-P. (2012). The connectome mapper: an open-source processing pipeline to map connectomes with MRI. *PloS One*, *7*(12), e48121.
Damoiseaux, J. S., & Greicius, M. D. (2009). Greater than the sum of its parts: a review of studies combining structural connectivity and resting-state functional connectivity. *Brain Structure & Function*, *213*(6), 525–533.
Deco, G., Ponce-Alvarez, A., Mantini, D., Romani, G. L., Hagmann, P., & Corbetta, M. (2013). Resting-state functional connectivity emerges from structurally and dynamically shaped slow linear fluctuations. *The Journal of Neuroscience: The Official Journal of the Society for Neuroscience*, *33*(27), 11239–11252.

de Haan, W., Mott, K., van Straaten, E. C. W., Scheltens, P., & Stam, C. J. (2012). Activity dependent degeneration explains hub vulnerability in Alzheimer's disease. *PLoS Computational Biology*, *8*(8), e1002582.

Desikan, R. S., Ségonne, F., Fischl, B., Quinn, B. T., Dickerson, B. C., Blacker, D., … Killiany, R. J. (2006). An automated labeling system for subdividing the human cerebral cortex on MRI scans into gyral based regions of interest. *NeuroImage*, *31*(3), 968–980.

Farahibozorg, S.-R., Henson, R. N., & Hauk, O. (2018). Adaptive cortical parcellations for source reconstructed EEG/MEG connectomes. *NeuroImage*, *169*, 23–45.

Finger, H., Bönstrup, M., Cheng, B., Messé, A., Hilgetag, C., Thomalla, G., … König, P. (2016). Modeling of large-scale functional brain networks based on structural connectivity from DTI: comparison with EEG derived phase coupling networks and evaluation of alternative methods along the modeling path. *PLoS Computational Biology*, *12*(8), e1005025.

Glomb, K., Ponce-Alvarez, A., Gilson, M., Ritter, P., & Deco, G. (2017). Resting state networks in empirical and simulated dynamic functional connectivity. *NeuroImage*, *159*, 388–402.

Goñi, J., van den Heuvel, M. P., Avena-Koenigsberger, A., Velez de Mendizabal, N., Betzel, R. F., Griffa, A., … Sporns, O. (2014). Resting-brain functional connectivity predicted by analytic measures of network communication. *Proceedings of the National Academy of Sciences of the United States of America*, *111*(2), 833–838.

Griffa, A., Alemán-Gómez, Y., & Hagmann, P. (2019). *Structural and functional connectome from 70 young healthy adults* [Data set]. https://doi.org/10.5281/zenodo.2872624

Hagmann, P., Cammoun, L., Gigandet, X., Meuli, R., Honey, C. J., Wedeen, V. J., & Sporns, O. (2008). Mapping the structural core of human cerebral cortex. *PLoS Biology*, *6*(7), e159.

Hall, E. L., Robson, S. E., Morris, P. G., & Brookes, M. J. (2014). The relationship between MEG and fMRI. *NeuroImage*, *102 Pt 1*, 80–91.

Hipp, J. F., Hawellek, D. J., Corbetta, M., Siegel, M., & Engel, A. K. (2012). Large-scale cortical correlation structure of spontaneous oscillatory activity. *Nature Neuroscience*, *15*(6), 884–890.

Honey, C. J., Sporns, O., Cammoun, L., Gigandet, X., Thiran, J. P., Meuli, R., & Hagmann, P. (2009). Predicting human resting-state functional connectivity from structural connectivity. *Proceedings of the National Academy of Sciences of the United States of America*, *106*(6), 2035–2040.

Jeurissen, B., Descoteaux, M., Mori, S., & Leemans, A. (2019). Diffusion MRI fiber tractography of the brain. *NMR in Biomedicine*, *32*(4), e3785.

Jones, D. K. (2010). Challenges and limitations of quantifying brain connectivity in vivo with diffusion MRI. *Imaging in Medicine*, *2*(3), 341–355.

Laird, A. R., Eickhoff, S. B., Li, K., Robin, D. A., Glahn, D. C., & Fox, P. T. (2009). Investigating the functional heterogeneity of the default mode network using coordinate-based meta-analytic modeling. *The Journal of Neuroscience: The Official Journal of the Society for Neuroscience*, *29*(46), 14496–14505.

Liu, Q., Ganzetti, M., Wenderoth, N., & Mantini, D. (2018). Detecting Large-Scale Brain Networks Using EEG: Impact of Electrode Density, Head Modeling and Source Localization. *Frontiers in Neuroinformatics*, *12*, 4.

Malmivuo, J. A., & Suihko, V. E. (2004). Effect of skull resistivity on the spatial resolutions of

EEG and MEG. *IEEE Transactions on Bio-Medical Engineering*, *51*(7), 1276–1280.

Medaglia, J. D., Lynall, M.-E., & Bassett, D. S. (2015). Cognitive network neuroscience. *Journal of Cognitive Neuroscience*, *27*(8), 1471–1491.

Meier, J., Tewarie, P., Hillebrand, A., Douw, L., van Dijk, B. W., Stufflebeam, S. M., & Van Mieghem, P. (2016). A Mapping Between Structural and Functional Brain Networks. *Brain Connectivity*, *6*(4), 298–311.

Michel, C. M., Murray, M. M., Lantz, G., Gonzalez, S., Spinelli, L., & Grave de Peralta, R. (2004). EEG source imaging. *Clinical Neurophysiology: Official Journal of the International Federation of Clinical Neurophysiology*, *115*(10), 2195–2222.

Musso, F., Brinkmeyer, J., Mobascher, A., Warbrick, T., & Winterer, G. (2010). Spontaneous brain activity and EEG microstates. A novel EEG/fMRI analysis approach to explore resting-state networks. *NeuroImage*, *52*(4), 1149–1161.

Nolte, G., Bai, O., Wheaton, L., Mari, Z., Vorbach, S., & Hallett, M. (2004). Identifying true brain interaction from EEG data using the imaginary part of coherency. *Clinical Neurophysiology: Official Journal of the International Federation of Clinical Neurophysiology*, *115*(10), 2292–2307.

O'Neill, G. C., Barratt, E. L., Hunt, B. A. E., Tewarie, P. K., & Brookes, M. J. (2015). Measuring electrophysiological connectivity by power envelope correlation: a technical review on MEG methods. *Physics in Medicine and Biology*, *60*(21), R271–R295.

Palva, J. M., Wang, S. H., Palva, S., Zhigalov, A., Monto, S., Brookes, M. J., … Jerbi, K. (2018). Ghost interactions in MEG/EEG source space: A note of caution on inter-areal coupling measures. *NeuroImage*, *173*, 632–643.

Pascual-Marqui, R. D., Biscay, R. J., Bosch-Bayard, J., Faber, P., Kinoshita, T., Kochi, K., … Yoshimura, M. (2017). Innovations orthogonalization: a solution to the major pitfalls of EEG/MEG "leakage correction." Retrieved from http://arxiv.org/abs/1708.05931

Pons, A. J., Cantero, J. L., Atienza, M., & Garcia-Ojalvo, J. (2010). Relating structural and functional anomalous connectivity in the aging brain via neural mass modeling. *NeuroImage*, *52*(3), 848–861.

Ponten, S. C., Daffertshofer, A., Hillebrand, A., & Stam, C. J. (2010). The relationship between structural and functional connectivity: graph theoretical analysis of an EEG neural mass model. *NeuroImage*, *52*(3), 985–994.

Preti, M. G., & Van De Ville, D. (2019). Decoupling of brain function from structure reveals regional behavioral specialization in humans. *Nature Communications*, *10*(1), 4747.

Rubega, M., Carboni, M., Seeber, M., Pascucci, D., Tourbier, S., Toscano, G., … Michel, C. M. (2019). Estimating EEG Source Dipole Orientation Based on Singular-value Decomposition for Connectivity Analysis. *Brain Topography*, *32*(4), 704–719.

Rubinov, M., & Sporns, O. (2010). Complex network measures of brain connectivity: uses and interpretations. *NeuroImage*, *52*(3), 1059–1069.

Schoffelen, J.-M., & Gross, J. (2009). Source connectivity analysis with MEG and EEG. *Human Brain Mapping*, *30*(6), 1857–1865.

Shuman, D. I., Narang, S. K., Frossard, P., Ortega, A., & Vandergheynst, P. (2012). The Emerging Field of Signal Processing on Graphs: Extending High-Dimensional Data Analysis to Networks and Other Irregular Domains. Retrieved from

http://arxiv.org/abs/1211.0053
Siems, M., Pape, A.-A., Hipp, J. F., & Siegel, M. (2016). Measuring the cortical correlation structure of spontaneous oscillatory activity with EEG and MEG. *NeuroImage*, *129*, 345–355.
Silfverhuth, M. J., Hintsala, H., Kortelainen, J., & Seppänen, T. (2012). Experimental comparison of connectivity measures with simulated EEG signals. *Medical & Biological Engineering & Computing*, *50*(7), 683–688.
Srinivasan, R., Winter, W. R., Ding, J., & Nunez, P. L. (2007). EEG and MEG coherence: measures of functional connectivity at distinct spatial scales of neocortical dynamics. *Journal of Neuroscience Methods*, *166*(1), 41–52.
Srinivasan, R., Winter, W. R., & Nunez, P. L. (2006). Source analysis of EEG oscillations using high-resolution EEG and MEG. *Progress in Brain Research*, *159*, 29–42.
Stam, C. J., Nolte, G., & Daffertshofer, A. (2007). Phase lag index: assessment of functional connectivity from multi channel EEG and MEG with diminished bias from common sources. *Human Brain Mapping*, *28*(11), 1178–1193.
Tadel, F., Baillet, S., Mosher, J. C., Pantazis, D., & Leahy, R. M. (2011). Brainstorm: a user-friendly application for MEG/EEG analysis. *Computational Intelligence and Neuroscience*, *2011*, 879716.
Tewarie, P., Abeysuriya, R., Byrne, Á., O'Neill, G. C., Sotiropoulos, S. N., Brookes, M. J., & Coombes, S. (2019). How do spatially distinct frequency specific MEG networks emerge from one underlying structural connectome? The role of the structural eigenmodes. *NeuroImage*, *186*, 211–220.
Tewarie, P., Hillebrand, A., van Dellen, E., Schoonheim, M. M., Barkhof, F., Polman, C. H., … Stam, C. J. (2014). Structural degree predicts functional network connectivity: a multimodal resting-state fMRI and MEG study. *NeuroImage*, *97*, 296–307.
Tognoli, E., & Kelso, J. A. S. (2009). Brain coordination dynamics: true and false faces of phase synchrony and metastability. *Progress in Neurobiology*, *87*(1), 31–40.
Tomasi, D., Wang, G.-J., & Volkow, N. D. (2013). Energetic cost of brain functional connectivity. *Proceedings of the National Academy of Sciences of the United States of America*, *110*(33), 13642–13647.
Tourbier, S., Aleman-Gomez, Y., Griffa, A., Bach Cuadra, M., & Hagmann, P. (2019). *connectomicslab/connectomemapper3: Connectome Mapper v3.0.0-beta-20190815*. https://doi.org/10.5281/zenodo.3475970
Uhlhaas, P. J., Pipa, G., Lima, B., Melloni, L., Neuenschwander, S., Nikolić, D., & Singer, W. (2009). Neural synchrony in cortical networks: history, concept and current status. *Frontiers in Integrative Neuroscience*, *3*, 17.
van Dellen, E., Hillebrand, A., Douw, L., Heimans, J. J., Reijneveld, J. C., & Stam, C. J. (2013). Local polymorphic delta activity in cortical lesions causes global decreases in functional connectivity. *NeuroImage*, *83*, 524–532.
Vincent, J. L., Patel, G. H., Fox, M. D., Snyder, A. Z., Baker, J. T., Van Essen, D. C., … Raichle, M. E. (2007). Intrinsic functional architecture in the anaesthetized monkey brain. *Nature*, *447*(7140), 83–86.
Wedeen, V. J., Hagmann, P., Tseng, W.-Y. I., Reese, T. G., & Weisskoff, R. M. (2005). Mapping

complex tissue architecture with diffusion spectrum magnetic resonance imaging. *Magnetic Resonance in Medicine: Official Journal of the Society of Magnetic Resonance in Medicine / Society of Magnetic Resonance in Medicine*, *54*(6), 1377–1386.

Wedeen, V. J., Wang, R. P., Schmahmann, J. D., Benner, T., Tseng, W. Y. I., Dai, G., … de Crespigny, A. J. (2008). Diffusion spectrum magnetic resonance imaging (DSI) tractography of crossing fibers. *NeuroImage*, *41*(4), 1267–1277.

Wens, V., Marty, B., Mary, A., Bourguignon, M., Op de Beeck, M., Goldman, S., … De Tiège, X. (2015). A geometric correction scheme for spatial leakage effects in MEG/EEG seed-based functional connectivity mapping. *Human Brain Mapping*, *36*(11), 4604–4621.

Whittingstall, K., Stroink, G., Gates, L., Connolly, J. F., & Finley, A. (2003). Effects of dipole position, orientation and noise on the accuracy of EEG source localization. *Biomedical Engineering Online*, *2*, 14.

Wirsich, J., Ridley, B., Besson, P., Jirsa, V., Bénar, C., Ranjeva, J.-P., & Guye, M. (2017). Complementary contributions of concurrent EEG and fMRI connectivity for predicting structural connectivity. *NeuroImage*, *161*, 251–260.

Yeo, B. T. T., Krienen, F. M., Sepulcre, J., Sabuncu, M. R., Lashkari, D., Hollinshead, M., … Buckner, R. L. (2011). The organization of the human cerebral cortex estimated by intrinsic functional connectivity. *Journal of Neurophysiology*, *106*(3), 1125–1165.